#### **RESEARCH ARTICLE**



# Extraction of Titanium, Aluminum, and Rare Earth Values from Upgraded Bauxite Residue

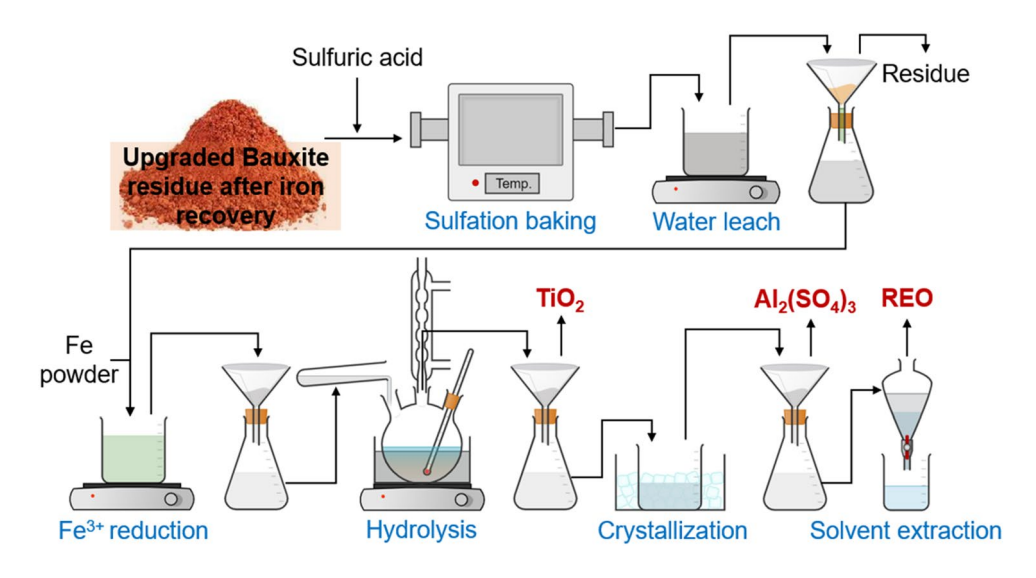
Himanshu Tanvar<sup>1</sup> · Brajendra Mishra<sup>1</sup>

Received: 29 September 2022 / Accepted: 18 March 2023 © The Minerals, Metals & Materials Society 2023

#### Abstract

The Bayer process for alumina production generates more than 160 million tons of bauxite residue annually. The current global stockpiles of bauxite residue have reached more than 4 billion tons with less than 2% annual recycling rate. Critical elements such as Sc and Y present an opportunity to explore bauxite residue as a secondary resource; however, low concentration affects the process economics. The following research focuses on the recovery of Ti, Al, and rare earth elements (Sc, Y, La, Ce) from upgraded bauxite residue obtained after Fe, Na, Ca, and Si separation. Recovery of major elements resulted in upgradation of Ti and RE values up to fourfold. Thermodynamic and kinetic aspects of the proposed recovery process are critically evaluated, and optimized conditions are reported to obtain high recovery of Ti, Al, and RE values. The major elements are recovered as high-purity (>99.5%) TiO<sub>2</sub> and Al<sub>2</sub>(SO<sub>4</sub>)<sub>2</sub>.14H<sub>2</sub>O, whereas Sc and Y are concentrated into a liquid solution for downstream recovery with solvent extraction.

#### **Graphical Abstract**



Keywords Bauxite residue · Scandium · Titanium · Sulfation

The contributing editor for this article was Atsushi Shibayama.

Published online: 30 March 2023

# Introduction

Aluminum is primarily produced by refining the bauxite ore to alumina in the Bayer Process, followed by electrolytic reduction to metal in Hall–Héroult process [1]. More than 95% of the global alumina production (134 million tons) in



<sup>☑</sup> Brajendra Mishra bmishra@wpi.edu

Material Science and Engineering, Worcester Polytechnic Institute, Worcester, MA 01609, USA

2021 was from bauxite processed through the Bayer process [2]. The global reserves of bauxite ore are estimated between 55 and 75 billion tons and are sufficient to meet the world demand well into the future [3]. Bayer process includes digestion of crushed bauxite in an alkali solution of sodium hydroxide, followed by solid–liquid separation to generate sodium aluminate liquor for alumina recovery and subsequently produces a residual slurry (bauxite residue/red mud). Depending on the mineralogy of the Bauxite ore, 0.5–2.2 tons of bauxite residue is generated to produce one ton of alumina [2]. The annual generation of bauxite residue is more than 160 million tons, with 3–4 billion tons stockpiled worldwide [2, 4].

Bauxite residue is characterized by high alkalinity (pH 10–12), fine particle size (80% passing 10 microns), multiple elements, and moisture (30–60%) content [5, 6]. Less than 4% of the bauxite residue is utilized globally as an additive in the building and construction industries, while the rest is stacked near the alumina refinery and presents an alarming waste disposal situation [4]. Bauxite residue consists of mixed phases of iron (Fe, 5–60%), aluminum (Al, 5–30%), titanium (Ti, 1-15%), calcium (Ca, 2-14%), silicon (Si, 5-50%), and sodium (Na, 1-15%) along with rare earth elements (REEs: Sc, Y, La, Ce; 0.001 –0.032%), gallium (Ga, 0.001-0.011%), and vanadium (V, 0.03-0.23%) as critical elements [4, 6, 7]. Depending on the geographic location of the mined bauxite ore, and processing parameters of the local alumina refineries, the mineralogy of bauxite residue varies drastically [8–10]. The multi-element waste presents a potential source for the recovery of different metallic values. The extraction potential of different elements from bauxite residue is reported in many literature works; however, industrial-scale processing is still limited [2]. The complex association of different elements, physical and chemical characteristics make the extraction process challenging and expensive.

Recovery of critical elements, including Sc, Ga, and V, from bauxite residue have gained significant interest recently considering the supply risk of these elements [11]. Direct leaching of bauxite residue in different mineral and organic acids results in the dissolution of multiple elements making the downstream separation difficult [12, 13]. Sulfation baking and roasting are reported to selectively recover REEs from bauxite residue due to the difference in decomposition temperature of REEs and impurity elements at high temperatures. The decomposition temperature of Fe, Al, and Ti sulfate is 500-550 °C, whereas that of Sc and Y is more than 700 °C. The process involves baking of bauxite residue with sulfuric acid (1-2 mL/g, 120-200 °C, 2-24 h) to generate metal sulfates and further decomposition of sulfates (except RE) at high temperatures (600-800 °C) and water leaching to dissolve REEs [14–17]. The process is not cost-effective due to the very low starting concentration of REEs and high acid requirement due to the presence of other metal ions. In an industrial setting, it will not be economically viable to convert all the elements in bauxite residue to sulfate form and subsequently decompose all the sulfates for recovery of 50–100 ppm RE. Furthermore, the recovery of a small fraction of elements does not reduce the volume burden of bauxite residue and will result in stockpiling another solid waste. Therefore, separating Fe from bauxite residue is essential to concentrate the content of valuable metals for downstream recovery.

The literature presents pyrometallurgical methods to recover Fe as pig iron or magnetite concentrate [18, 19]. Reduction roasting reduces hematite in bauxite residue to magnetite, and subsequent magnetic separation results in a magnetic concentrate. The magnetic separation product is not ideal and provides low separation efficiency (47-60% Fe grade, 70-80% Fe recovery) due to the formation of mixed oxides (fayalite, hercynite) [19, 20]. Smelting of bauxite residue with reductant (carbon) at a high temperature (1500-1600 °C) in an induction furnace results in the separation of Fe into metallic form and subsequently produces a slag [21, 22]. Generally, CaO (10–20 wt.%)-based flux is added during the smelting process to generate optimal slag for good separation and fluidity. Recovery of Al and REEs from slag is reported based on hydrometallurgical methods; however, the addition of flux during smelting dilutes the concentration of these elements and are not significantly upgraded in the slag compared to raw bauxite residue [18, 23, 24]. Furthermore, economic uncertainty due to high energy consumption in smelting is the limiting factor for industrial-scale applications [25, 26]. Anawati et al. recently reported a two-stage process, where bauxite residue is first subjected to carbothermic reduction at 1600 °C to recover > 95% of Fe as metallic Fe and concentrate the Sc values in the slag. The resulting slag was subjected to sulfation baking using 1.25 g sulfuric acid per gram residue at 150 °C for 2 h and resulted in dissolution of 90% Sc and 47% Al [27].

In our previous work, a two-stage leaching process with hydrochloric acid and oxalic acid was reported for selective recovery of Fe in the form of high-purity magnetite from bauxite residue [28]. The previous process generated a residue consisting of Ti and RE with a concentration upgrade up to fourfold. The present study is focused on the recovery of Ti, RE (Sc, Y, La, Ce), and Al from the following residue. The proposed process is based on sulfation baking and leaching for the dissolution of metal values. Downstream separation of dissolved elements is performed with hydrolysis, crystallization, and solvent extraction to recover high-purity products. The process chemistry is briefly elucidated based on kinetic and thermodynamic analysis, followed by experimental evaluation and validation. The proposed process provides better selectivity, high recovery rate, and



purity of the final product and results in large volume utilization of bauxite residue with value recovery.

#### **Materials and Methods**

## **Sample Information**

The bauxite residue sample used in this study was procured from an alumina refinery (Rio Tinto Alcan) in Quebec City, Canada. The bauxite residue was processed through a hydrometallurgical process described in our previous work to separate and recover Fe as high-purity magnetite (Fig. 1). The process includes neutralization of bauxite residue with mild HCl followed by selective leaching of Fe in the form of ferric oxalate using oxalic acid. The oxalic leach liquor was further subjected to photochemical reduction to generate a ferrous oxalate precursor for magnetite production. The purity of the final magnetite product was more than 99%, with a recovery of approx. 89% Fe. The solid residue collected after separating major elements is used as the starting material in this study and constitutes about 26 wt.% of the raw bauxite residue. The chemical composition of raw bauxite residue and residue after the first stage of treatment is shown in Table 1. The starting material (referred to as residue throughout the manuscript) consists of 10.36% Si, 15.05% Ti, 8.9% Fe, and 13.85% Al along with 86.1 ppm Sc, 289.0 ppm Y, 24.2 ppm La, and 43.69 ppm Ce. The key mineral phases identified from XRD analysis include anatase (TiO<sub>2</sub>), rutile (TiO<sub>2</sub>), boehmite (AlOOH), and silica (SiO<sub>2</sub>). The upgradation process resulted in the separation of 99.8% Ca, 99.9% Na, 89.2% Fe, 46.2% Si, and 65.7% Al. The recovery of Sc in liquid solution during the processing was approx. 14.2%, while La and Ce were 81.6% and 93.6%, respectively. It is noteworthy that the Ti, Sc, and Y values were upgraded up to threefold—fourfold in the residue after the recovery of major elements.

## **Experimental Procedure**

Figure 1 shows a schematic for the experimental procedure followed in this work. The residue collected after the recovery of Fe was subjected to sulfation baking using sulfuric acid. The solid samples were thoroughly mixed with the desired amount of sulfuric acid (0.5–1.5 mL/g) to form a paste which was further transferred into a ceramic boat and heated in a tubular furnace at 150–400 °C for 0.5–2 h. The sulfated sample was pulverized using a mortar and pestle and

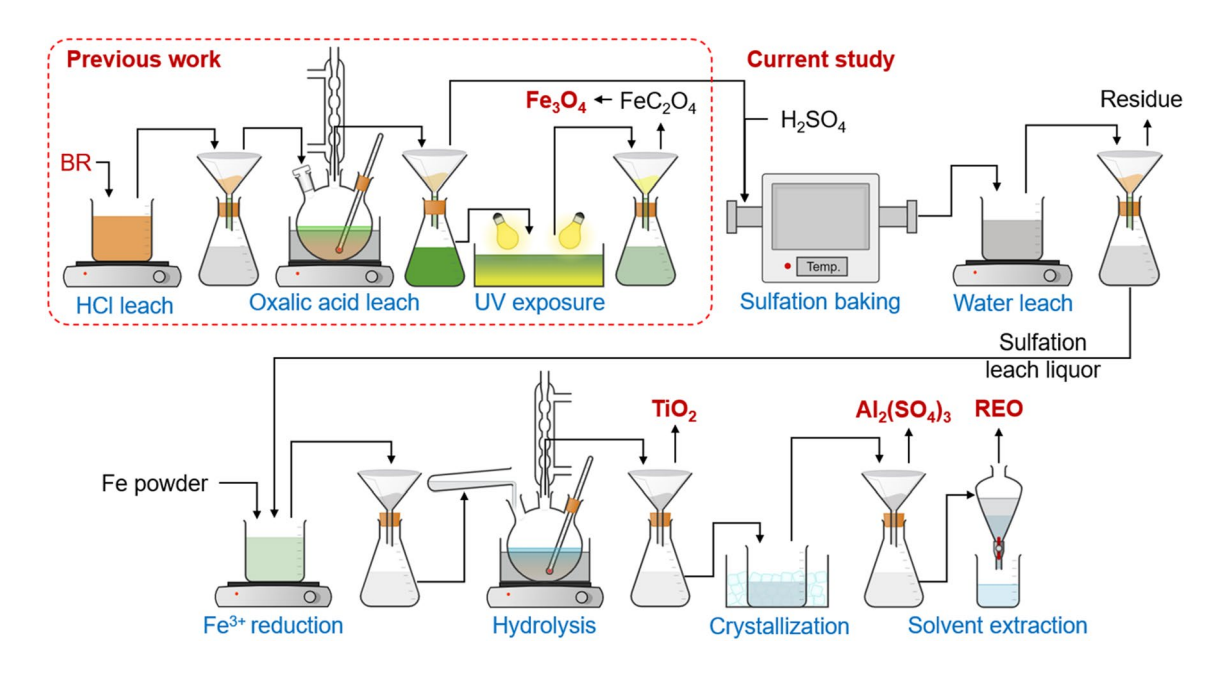


Fig. 1 Process flowsheet followed in this study

**Table 1** Chemical analysis of bauxite residue and upgraded residue after magnetite recovery (\* ppm)

Element (wt.%)	Ca	Si	Ti	Na	Fe	Al	Sc*	Y*	La*	Ce*
Bauxite residue	2.31	5.01	3.67	6.98	21.44	10.21	36.84	62.25	34.30	178.50
Upgraded residue	0.01	10.36	15.05	0.01	8.91	13.85	86.14	289.01	24.20	43.69
Extraction (%)	99.89	46.24	_	99.96	89.19	64.73	14.22	_	81.66	93.64



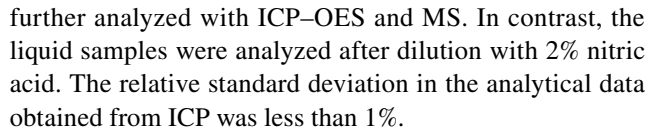
leached in 0.5 M sulfuric acid at 65 °C for 90 min. Leaching experiments were carried out in a 500 mL Pyrex beaker using a magnetic stirrer at 800 rpm. The leach residue and leach liquor were separated using a vacuum filter, followed by processing of leach liquor for recovery of Ti, Al, and RE. Majority of the experiments were performed twice, and average values are reported.

The selective precipitation of Ti was carried out using thermal hydrolysis, described as the Blumenfeld method in the literature [29, 30]. The leach liquor was contacted with Fe powder (stoichiometric dosage, 500 rpm mixing, 30 min) to reduce Fe<sup>+3</sup> to Fe<sup>+2</sup> and prevent coprecipitation. Hydrolysis experiments were carried out in a 1000 mL Pyrex flask connected to a condenser to avoid water loss during boiling. An appropriate amount (100 mL) of water and leach liquor was introduced into separate flasks and heated to 95 °C. When the solution reached the desired temperature, the leach liquor was transferred dropwise to the boiling water vessel. The reaction mixture was heated for 30 min to the first boiling point (105 °C). After that, the heating was turned off for 30 min to initiate aging, and further boiled to the so-called second boiling point (105–110 °C) for 2.5 h, then cooled down to room temperature before solid-liquid separation. Aliquots were withdrawn from the reactor at the desired time interval during hydrolysis to analyze the extraction behavior. Hydrolyzed Ti precipitate was collected after filtration using a vacuum filter and dried in a laboratory oven at 98 °C for 12 h.

The pH of the liquid solution after hydrolysis was adjusted to approx. 1.5–2 using ammonium hydroxide followed by crystallization of Al sulfate. Crystallization experiments were carried out by boiling the solution to saturation, followed by cooling to – 5 °C to crystallize aluminum sulfate (Al<sub>2</sub>(SO<sub>4</sub>)<sub>3</sub>.14H<sub>2</sub>O). The leach liquor was further collected and subjected to solvent extraction for recovery of REEs. Solvent extraction experiments were performed using three different extractants (10 vol.% D2EHPA, Cyanex 272, and Cyanex 572) to determine the selectivity and efficiency of RE recovery. The experiments were performed with an O/A ratio of 1:1 for 15 min at 800 rpm stirring speed. The aqueous and organic phases were separated after centrifuging the mixture at 4000 rpm for 5 min, followed by analysis of the aqueous phase to determine the extraction efficiency.

#### **Analytical Techniques**

The chemical analysis of the samples was carried out using Inductively Coupled Plasma–Optical Emission Spectroscopy (ICP–OES; PerkinElmer Optima 8000) and Mass Spectroscopy (MS; PerkinElmer NEXION350x). ICP–OES was used to analyze major elements, while ICP–MS for trace elements. Solid samples were fused with borate flux at 1000 °C for 1 h, dissolved in 25% nitric acid solution, diluted, and



Mineral phases present in the solid samples at different stages were determined using an X-ray diffractometer (XRD; PANalytical Empyrean). The diffraction data were measured using a Cr –  $K_{\alpha}$  radiation in the 2 – theta range of 10 to 80°, with a scanning rate of 2°/min and a step size of 0.02°. Thermodynamic information and standard Gibbs free energy of different reactions were determined using the Reaction module in FactSage 8.0.

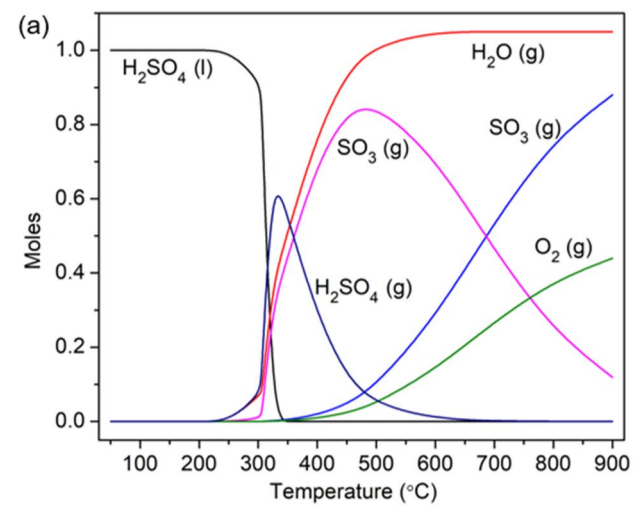
## **Results and Discussion**

## **Thermodynamic Analysis**

Sulfation baking is a solid-state reaction that is highly dependent on the decomposition behavior of sulfuric acid at high temperatures and its reactivity. Figure 2a shows the stability diagram of sulfuric acid in the temperature range of 25-900 °C calculated using thermodynamic database of FactSage software. Sulfuric acid decomposes to SO<sub>3</sub> and H<sub>2</sub>O in the temperature range of 127–427 °C. Some amount of gaseous sulfuric acid is also formed. The second stage of decomposition involves endothermic reduction of SO<sub>3</sub> to SO<sub>2</sub> and is observed at a temperature of more than 750 °C [31]. The main advantage of sulfation baking over direct leaching includes reduced acid demand, high reaction rate, and fast reaction kinetics. Figure 2b shows the underlying chemical reactions and standard Gibbs free energy for the reaction of different elements with sulfuric acid. The thermodynamic data show that the reaction is thermodynamically favored, where TiO<sub>2</sub> forms both Ti(SO<sub>4</sub>)<sub>2</sub> and TiOSO<sub>4</sub> phases, with Ti(SO<sub>4</sub>)<sub>2</sub> being more thermodynamically stable. Furthermore, the reaction of Fe<sub>2</sub>O<sub>3</sub> and Al<sub>2</sub>O<sub>3</sub> is more favorable at high temperatures compared to TiO<sub>2</sub>.

The mass transfer between solid and sulfuric acid increases with temperature and accelerates the reaction kinetics. Anatase and rutile (TiO<sub>2</sub>) phases are chemically inert compared to ilmenite (FeTiO<sub>3</sub>) and do not readily dissociate during industrial processing of ilmenite ore using sulfuric acid leaching [32, 33]. The inertness of the TiO<sub>2</sub> phase during sulfuric acid leaching is due to the underlying crystal structure consisting of TiO<sub>6</sub> octahedra, in which each Ti ion is in coordination with six oxygen ions located in the octahedral system. The crystal structure consists of a densely packed oxygen ion plane parallel to the quadruple axis of rutile crystal like a spinel structure and is rigid [33]. The breakage of the –Ti–O–Ti– bond induces deformation in the crystal lattice due to the difference in ionic radii of SO<sub>4</sub><sup>2-</sup> (0.258 nm) and O<sup>2-</sup> (0.163 nm). The large positive





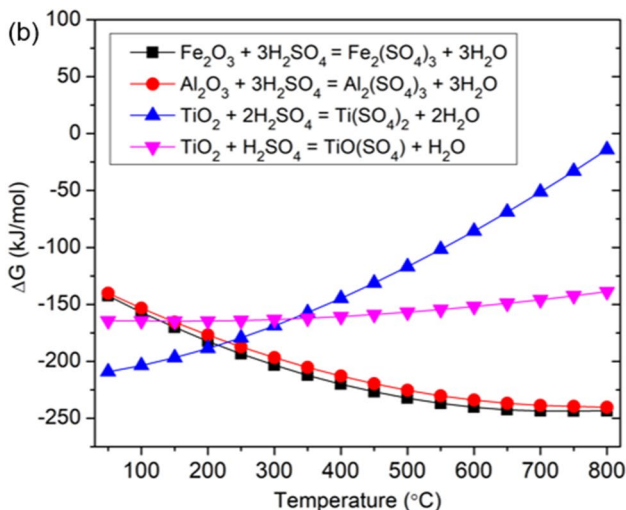


**Fig. 2** Thermodynamics of the underlying reactions: (a) Equilibrium concentration obtained from thermal decomposition of 1 mol  $\rm H_2SO_4 + 0.05$  mol  $\rm H_2O$ , (b) Gibbs free energy for reaction of different oxides with  $\rm H_2SO_4$ 

charge of Ti(IV) and its relatively large radii than other metal ions (such as Fe, Al) increases the activation energy of the substitution reaction of oxygen ions with other ligands ( $SO_4^{2-}$ ). Therefore, high temperature is required to meet the additional energy requirement for TiO<sub>2</sub> phase dissociation.

Figure 3 shows the thermogravimetric analysis (TGA) of the mixture of sulfuric acid and residue (upgraded feed). TGA analysis was performed at 25–800 °C temperature, with a heating rate of 9 °C/ min. There is no apparent weight loss until 110 °C, followed by continuous weight loss of 29.7% up to 274 °C. Rapid loss in weight was observed in the temperature range of 207–274 °C depicting the completion of the sulfation reaction. Additional weight loss of 4% was observed up to 540 °C, followed by rapid weight loss of 30% at 785 °C, corresponding to the decomposition of sulfates. The sulfates of Fe, Ti, Al, and Sc start to decompose

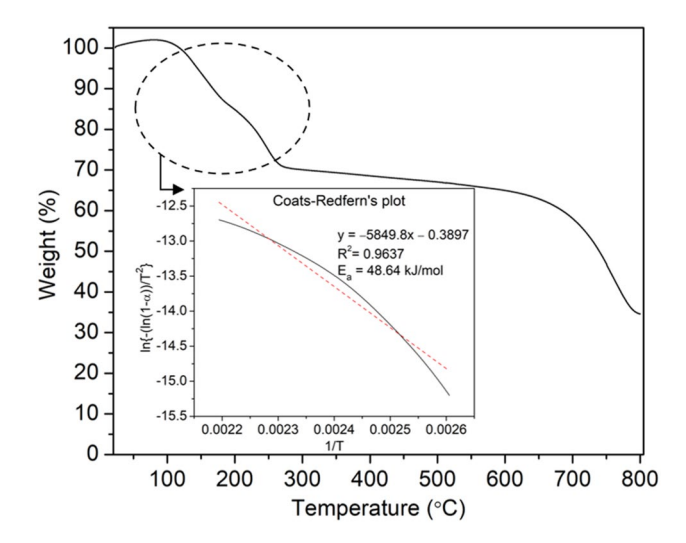


Fig. 3 TGA of residue and sulfuric acid mixture

to respective oxides at a temperature above 545 °C, 430 °C, 524 °C, and 700 °C [16]. The kinetic parameters and activation energy of the decomposition reaction were determined from TGA data by Coats-Redfern method [34]. The kinetic relation used is shown in Eqs. (1-2), where  $\alpha$  is the degree of conversion (mass loss) at time t, n is the reaction order, A is the Arrhenius preexponential factor ( $s^{-1}$ ),  $E_a$  is activation energy (kJ/mol), T is the temperature (K), and  $\beta$  is the heating rate (K/min). The model equation was plotted with 1/T on the abscissa. The value of n was adjusted between 0.1 and 1 to obtain the highest linear correlation coefficient using the least square method. The best fitting for the model was found using Eq. (1), with the value of n being 1. The activation energy determined from the straight-line slope was found as 48.64 kJ/mol and was further validated with experimental analysis.

$$\ln \left\{ \frac{-\ln(1-\alpha)}{T^2} \right\} = \ln \left( \frac{AR}{\beta E_a} \right) - \frac{E_a}{RT} (when n = 1)$$
 (1)

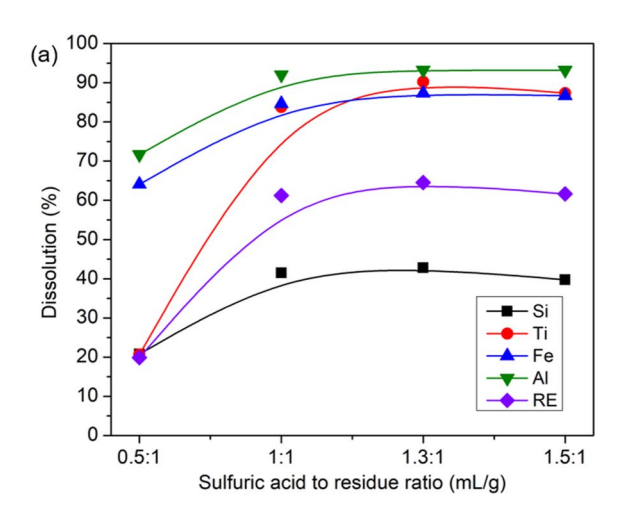
$$\ln\left\{\frac{1-(1-\alpha)^{1-n}}{T^2(1-n)}\right\} = \ln\left(\frac{AR}{\beta E_a}\right) - \frac{E_a}{RT}(when n \neq 1)$$
(2)

## **Sulfation Baking and Leaching**

The sulfation baking process was experimentally investigated to determine the optimal conditions and analyze the reaction mechanism. The acid demand based on stoichiometric calculations for the complete conversion of oxides to sulfates is 1.1 mL per gram of solid residue. The residue was thoroughly mixed with different amounts of sulfuric



acid (0.5 to 1.5 mL/g) and subjected to sulfation at 250 °C for 2 h. Figure 4a shows the dissolution results for different elements at variable acid to residue ratios. The dissolution percentage of different REEs (Sc, Y, Ce, Eu) was almost consistent; therefore, the dissolution of RE is shown as the combined dissolution of Sc, Y, Ce, and La. With an increase in acid dosage from 0.5 mL/g to 1 mL/g, the dissolution percentage of all elements increased. The highest recovery was obtained at acid to residue ratio of 1.3 mL/g resulting in 42.7% Si, 90.2% Ti, 87.3% Fe, 93.2% Al, and 64.5% RE dissolution. The dissolution of RE was limited to 65%, even at a high acid dose. Furthermore, the acid dosage was fixed at 1.3 mL/g while the temperature was varied between 150 and 400 °C at a constant heating time of 2 h. Figure 4b shows the dissolution data and weight loss values at different temperature conditions. A rapid increase in dissolution and weight loss was observed in the temperature range of 150-300 °C. At 300 °C approx. 34% weight loss was



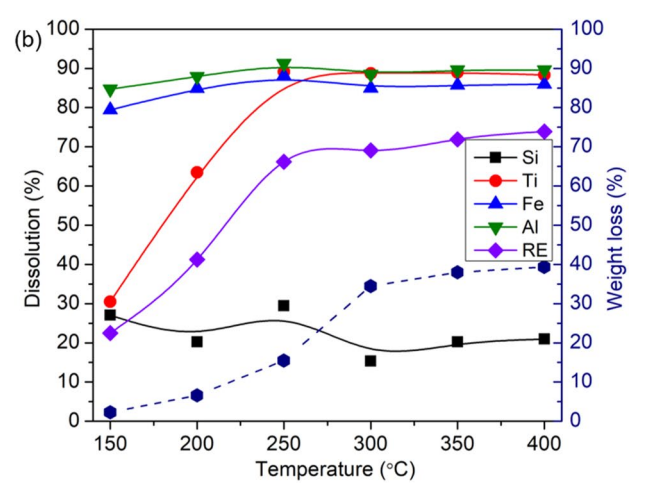


**Fig. 4** Dissolution value at different sulfation conditions (a) Effect of sulfuric acid to residue ratio at 250 °C for 2 h, (b) Effect of temperature at 1.3:1 mL/g acid to residue ratio for 2 h

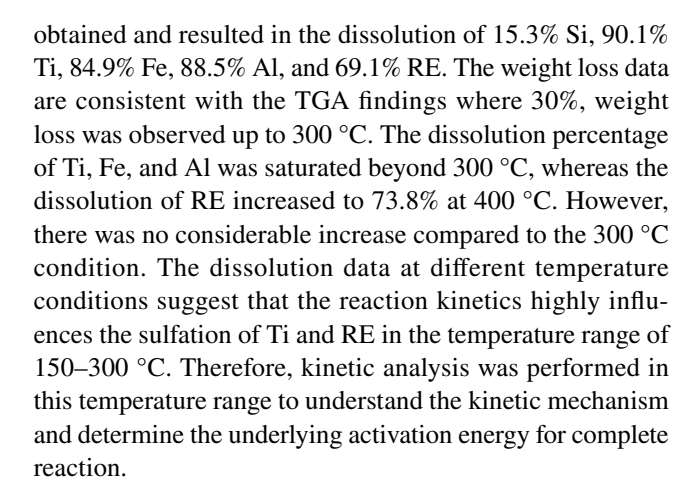


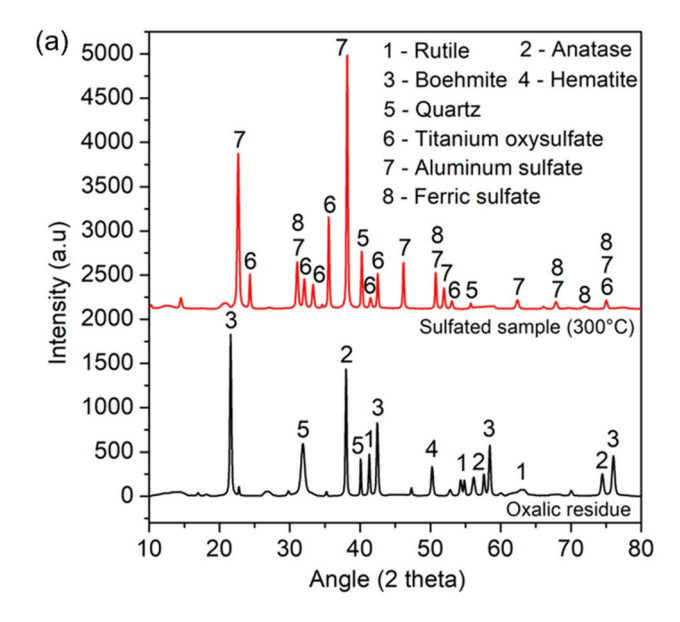
Figure 5a shows the XRD analysis of starting material and sulfated sample (1.3 mL acid per g residue, 300 °C). The XRD data show that anatase, rutile, boehmite, and hematite phases converted to respective sulfates after their reaction with sulfuric acid. No apparent rutile, anatase, and boehmite peaks were observed in the XRD of the sulfated sample. Figure 5b shows the XRD analysis of the final residue obtained at different temperature conditions. The peaks corresponding to rutile and anatase were found in the samples sulfated at 150, 200, and 250 °C showing incomplete dissociation. The peak intensity of unreacted phases in residue decreased from 150 °C to 250 °C and further disappeared at 300 °C. The XRD analysis of the final residue at a temperature higher than 300 °C shows the presence of quartz as the primary phase.

## **Kinetic Analysis of Sulfation**

Figure 6 shows the dissolution of different elements at various time and temperature conditions using 1.3 mL acid per gram residue. The dissolution percentage of Ti and RE is variable between 10–90% and 22–80%, whereas Fe, Al, and Si dissolution are limited to 75–85%, 85–95%, and 25–34%, respectively. The correlation plot of RE and Ti dissolution, shown in Fig. 6c, reflects a linear relationship ( $R^2$ =0.963) in the recovery of both elements. It can be interpreted that the RE values in the current bauxite residue are associated with Ti phases and result in parallel extraction.

Experimental results were fitted with the standard kinetic models to analyze the solid-state chemical reaction mechanism for Ti and RE extraction. The heat treatment mechanism is usually controlled by reaction at the interface or by diffusion of reactant through the product layer. Equation (3–5) shows the kinetics equations describing these mechanisms. Jander proposed the mechanism for diffusion-controlled reactions based on the parabolic rate law. In contrast, Ginstling and Braunshtein's model described the parabolic rate law, which relates the growth of the product layer to the decrease in interface area and can be applied to reactions controlled via gaseous





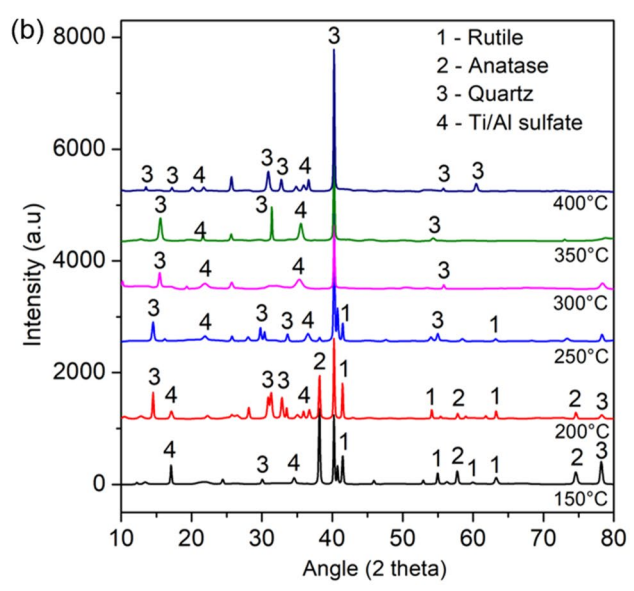


Fig. 5 XRD analysis (a) Oxalic residue and sulfated sample, (b) Leach residue at different temperature conditions

diffusion through the product layer. Considering the decomposition behavior of sulfuric acid at high temperatures and the possibility of reaction of both liquid and gaseous sulfuric acid, the standard kinetic models shown in Eqs. (3–5) were used for analysis.

Chemical reaction controlled:
$$X = k_f t$$
 (3)

Diffusioncontrolled(Jander): 
$$\left[1 - (1 - X)^{\frac{1}{3}}\right]^2 = k_r t$$
 (5)

Table 2 shows the correlation coefficient (R<sup>2</sup>) for different kinetic models investigated. The low  $R^2$  value (<0.75) at 300 °C reflects that the reaction is not kinetically limited at a temperature higher than 250 °C; therefore, the data points corresponding to 300 °C were not included in the Arrhenius plot. The diffusion-controlled model's overall fit was better than the chemical reaction-controlled model in the temperature range of 150–250 °C. Among the different diffusioncontrolled models investigated, the Jander model fits well with the experimental data providing the highest correlation coefficients. Figure 7a and b shows the best-fit differential model equation graphs of Ti and RE, corresponding to the diffusion mechanism based on the Jander model. The linear data fitting was performed to determine the line equation and obtain the reaction rate constant represented by the slope. The activation energy was further calculated using the standard Arrhenius plot (natural logarithm of the reaction rate versus the reciprocal of absolute temperature). Figure 7c and d represents the Arrhenius plot for Ti and Sc dissolution. The activation energy for recovery of Ti and Sc was determined as 55.67 kJ/mol and 42.11 kJ/mol, respectively. The experimentally determined activation energy is in close agreement with the value obtained from TGA data using the Coats-Redfern method (48.64 kJ/mol).

# **Recovery of Metal Values from Solution**

The leach solution obtained after sulfation roasting and water leaching at optimized conditions (300 °C, 1.3 mL/g acid, 1 h) consist of 15.23 g/L Ti, 10.36 g/L Al, 10.36 g/L Fe, 0.13 g/L Si, and 0.03 g/L RE. Based on the standard Pourbaix diagram, Al and RE are soluble as trivalent ions up to a pH value of 4–5, whereas Fe in its ferrous oxidation state (Fe<sup>2+</sup>) is soluble in a broad pH range from highly acidic to a mildly alkaline solution. In contrast, ferric ion (Fe<sup>3+</sup>) is soluble only in the acidic range (pH < 3) with oxidizing conditions (Eh > 0.7 V) (Monhemius, 2017). To selectively recover Ti from sulfate leach solution, Fe(III) was first reduced to Fe(II) using Fe filings to prevent coprecipitation of Fe(OH)<sub>3</sub>. The hydrolysis experiments without Fe reduction resulted in the contamination of Ti product with high amounts of Fe impurities. Figure 8a

Diffusion controlled (Ginstling and Braunshtein): 
$$1 - \frac{2}{3}X - (1 - X)^{\frac{2}{3}} = k_d t$$
 (4)

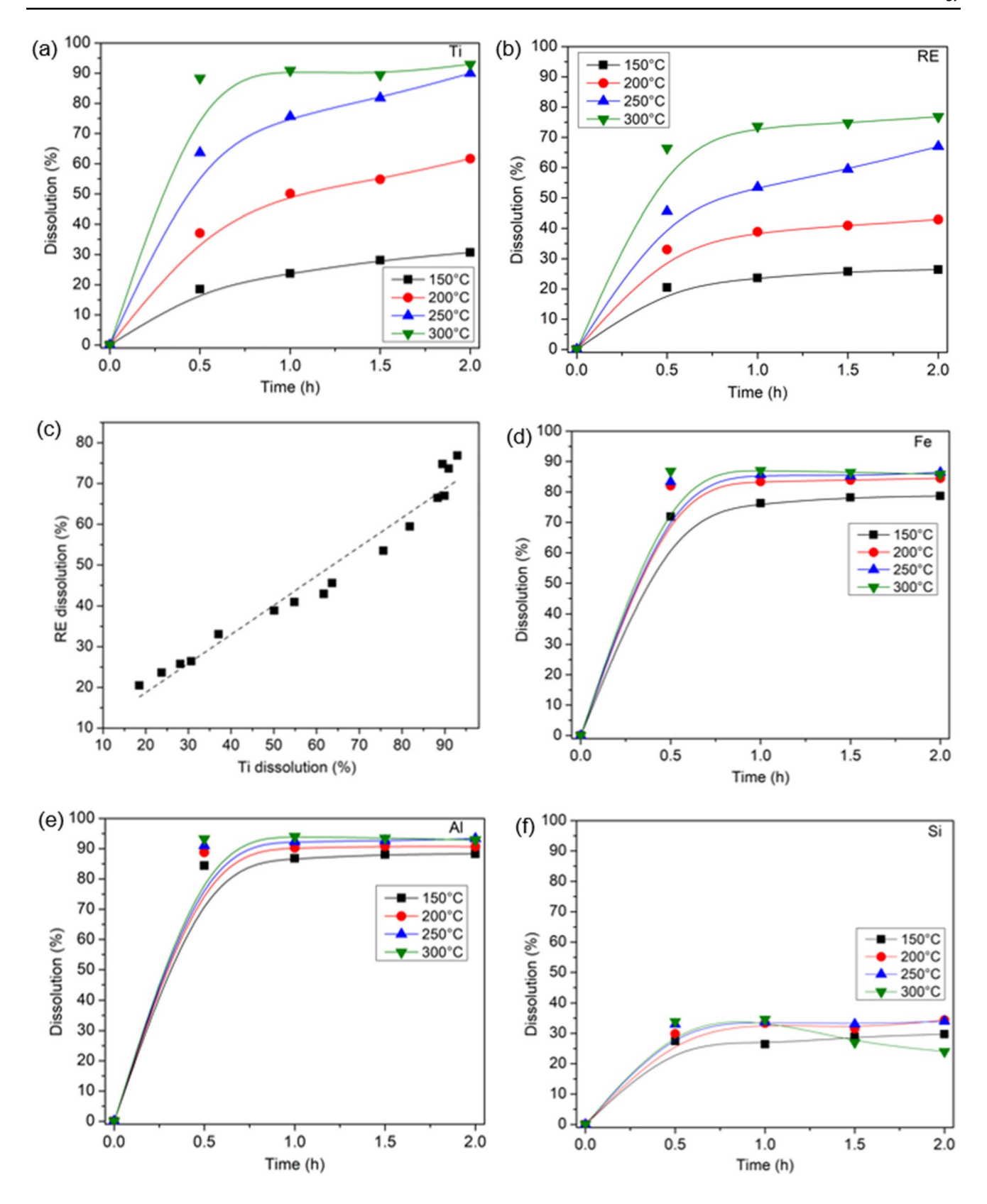


Fig. 6 Effect of time and temperature on dissolution of different elements: (a) Ti, (b) Sc, (c) Ti vs Sc, (d) Fe, (e) Al, and (f) Si



**Table 2** Correlation coefficient (R<sup>2</sup>) values for data fitting using different model equations

Kinetic model	Element	150 °C	200 °C	250 °C	300 °C
Chemical reaction controlled	Ti	0.8446	0.8305	0.7533	0.5338
	Sc	0.6965	0.6934	0.7836	0.6082
Diffusion controlled (G-B model)	Ti	0.9868	0.9862	0.9802	0.6249
	Sc	0.8526	0.8603	0.9743	0.7633
Diffusion controlled (Jander model)	Ti	0.9898	0.9914	0.9867	0.6697
	Sc	0.8595	0.8731	0.9830	0.7973

shows the concentration of different elements in solution as a function of time during hydrolysis of Ti. The concentration of Fe, Al, Si, and RE remained constant, reflecting no precipitation, whereas the concentration of Ti went down from 15.23 g/L to 3.86 g/L within 1 h, resulting in 74.6% Ti extraction. The final concentration of Ti after 5 h was 1.35 g/L, corresponding to 91.12% Ti extraction.

Cooling crystallization of the supersaturated solution after Ti separation resulted in approx. 94.5% Al recovery and the final solution consists of 0.72 g/L Ti, 0.71 g/L Al, 10.92 g/L Fe, 0.11 g/L Si, and 0.03 g/L RE. Figure 8b shows the XRD analysis of Ti and Al products. The Ti product consisted of a mixture of anatase and rutile phases, whereas the Al product is mainly composed of Al<sub>2</sub>(SO<sub>4</sub>)<sub>3</sub>.14H<sub>2</sub>O. The SEM and chemical analysis of Ti and Al products are shown in Fig. 9a and b. The Ti precipitate is composed of sub-micron-sized spherical particles agglomerated together, whereas the Al sulfate crystals (alum) show the presence of flaky particles of variable sizes. The chemical analysis shows that the Ti precipitate and Al sulfate crystals are characterized by purity of more than 99% and can be directly used as a material for industrial applications.

The solution obtained after Ti and Al recovery is mainly composed of 10.92 g/L Fe as a major impurity along with 6.46 ppm Sc, 17.91 ppm Y, 198 ppm Ce, and 0.85 ppm La as valuable components. The dissolved RE can be further recovered as a mixed concentrate from the purified solution using solvent extraction. It is expected that the presence of Fe(II) in the solution will restrict the extraction of Fe into the organic phase due to low charge density resulting in selective recovery of REEs. Feasibility tests for solvent extraction were carried out using three commercially available extractants (D2EHPA, Cyanex 272, Cyanex 572) at an organic-to-aqueous (O/A) phase ratio of 1:1 for 15 min. The experimental trials were conducted with 10 vol.% extractants diluted in kerosene. Figure 10 shows the extraction behavior of different elements

using different organic extractants. The highest extraction of RE was obtained with D2EHPA and resulted in the recovery of 89.1% Sc, 77.2% Y, 78.2% Ce, and 82% La. Additionally, only 3.1% Fe, 4.9% Al, 3.2% Si, and 15. 3% Ti were extracted as impurities. Cyanex 272 was better than Cyanex 572 in terms of higher RE extraction. Preliminary analysis of the solvent extraction process shows positive results with high selectivity toward extraction of Sc, Y, La, and Ce from the leach solution. The following results present a baseline for further optimization of the solvent extraction process to determine the required extractant concentration, O/A phase ratio, and the number of stages for the counter-current extraction process.

#### **Overall Flowsheet**

Recycling metals from complex waste streams cannot be achieved in a single process step and requires a combination of different unit operations based on pyro- and hydrometallurgy technologies. Figure 11 shows a comprehensive flowsheet with material balance for recovery of different metallic oxides from bauxite residue. The upgradation of bauxite residue is carried out based on our previous work and resulted in the recovery of magnetite, alumina, calcium carbonate, and silica [35]. The current work reports on the recovery of Ti, Al, and RE from upgraded residue using sulfation baking and leaching process. Upgradation of bauxite residue provided a fourfold increase in the concentration of Ti and RE, reducing the acid demand during sulfation and providing better selectivity during recovery from solution. Ti and Al are recovered as high-purity TiO2 and  $Al_2(SO_4)_3$  after hydrolysis and crystallization of leach solution. The leach solution containing 6.46 ppm Sc and 17.91 ppm Y was further subjected to solvent extraction with D2EHPA and provided high selectivity toward the extraction of RE.

The following research combined with our previous work presents a comprehensive flowsheet for recovery of multiple valuable metallic oxides from bauxite residue and provides a high-volume utilization of bauxite residue. The final residue



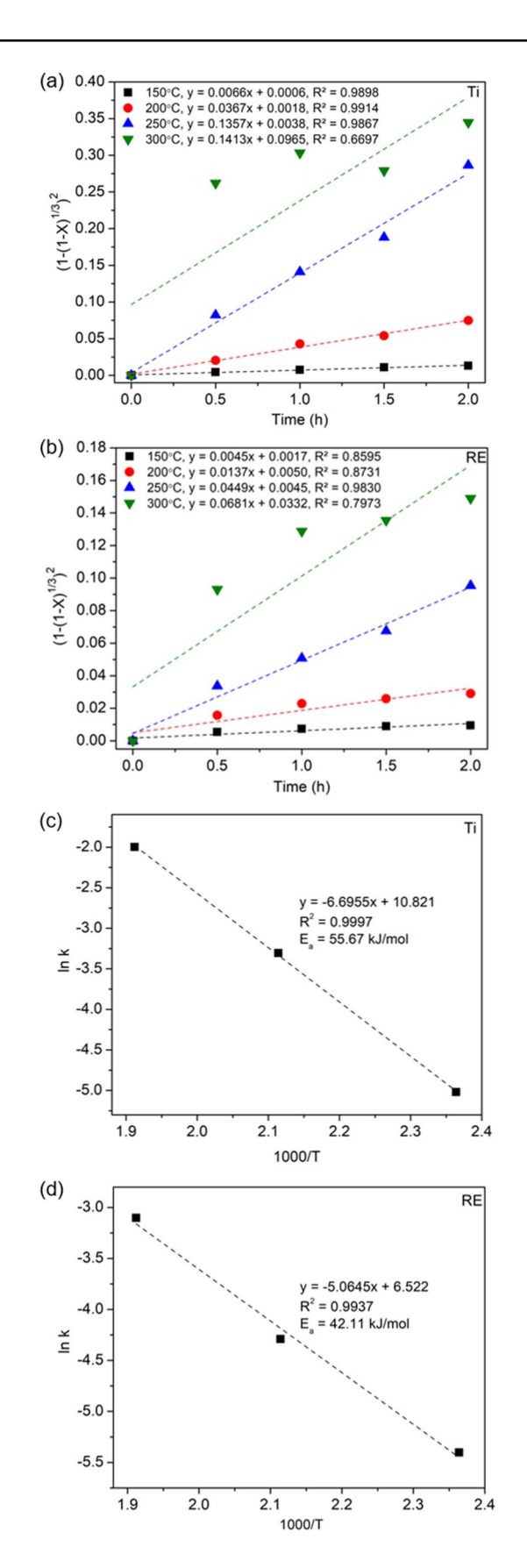


Fig. 7 Differential model equation graphs for (a) Ti, (b) Sc and Arrhenius plot for (c) Ti, (d) Sc



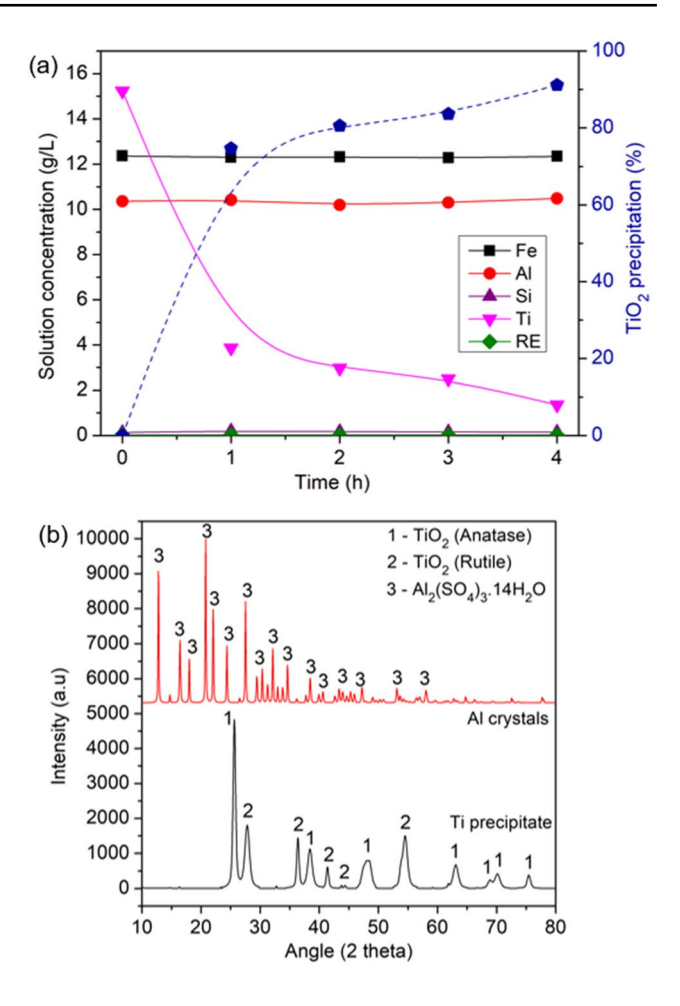


Fig. 8 a Behavior of different elements during thermal hydrolysis, b XRD analysis of TiO<sub>2</sub> precipitate and Al<sub>2</sub>(SO<sub>4</sub>)<sub>3</sub>.14H<sub>2</sub>O crystals

constitutes to only 10.9 wt.% of the starting material and contains more than 70% quartz. The recovery of Sc and Y along-side major elements (Fe, Al, Ti) provides an opportunity to utilize bauxite residue as a multi-element resource. Sc is the most critical element present in bauxite residue; however, the low concentration (10–30 ppm) yields less product (15–20 g  $Sc_2O_3$  from 1-ton bauxite residue) at the expense of expensive reagents; therefore, recovery of RE as a byproduct of the base metal recovery process will favor the process economics.

## **Conclusion**

The following work presents an in depth analysis of the sulfation baking process to recover Ti, Al, and RE (Sc, Y, La, Ce) from upgraded bauxite residue. In the first

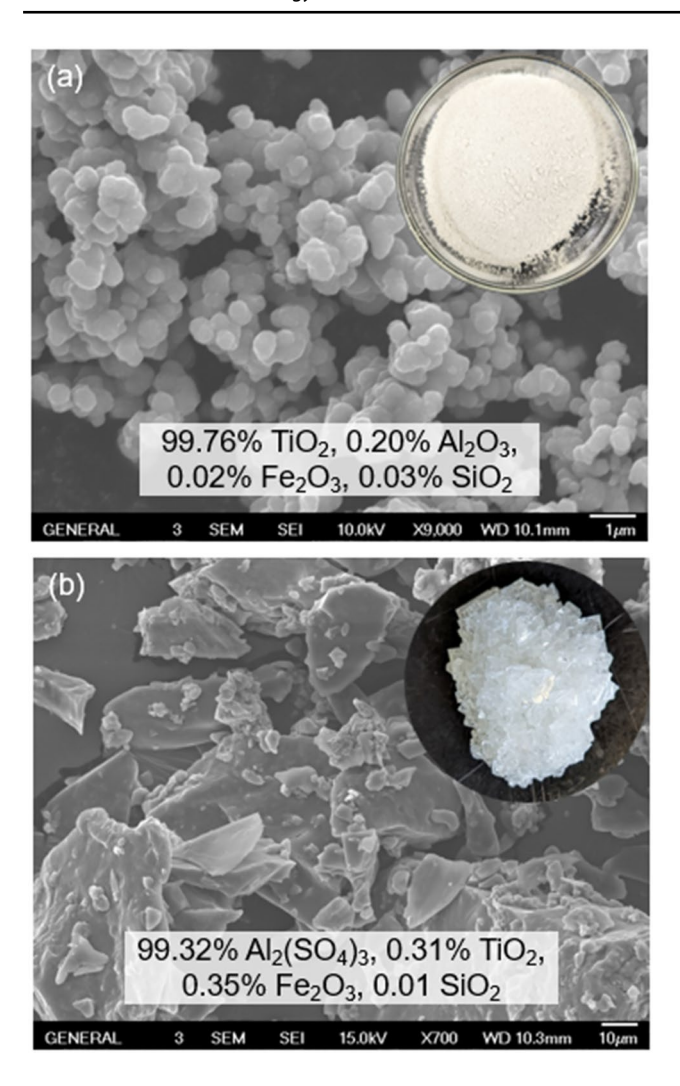
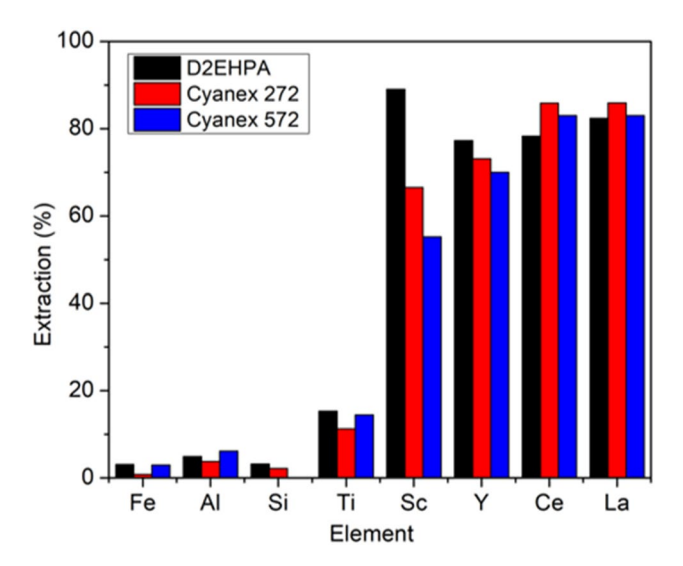


Fig. 9 SEM and chemical analysis of (a)  $TiO_2$  precipitate, (b)  $Al_2(SO_4)_3.14H_2O$  crystals



**Fig. 10** Extraction behavior of different elements during solvent extraction of RE using different organic extractants

stage of treatment, bauxite residue was subjected to twostage acid leaching using hydrochloric and oxalic acid, which resulted in 89.2% Fe, 99.8% Ca, 99.9% Na, 46.2% Si, and 65.7% Al extraction. The preprocessing resulted in upgraded bauxite residue (26 wt.% of starting material) containing of Ti, Sc, and Y values upgraded up to fourfold. The separation and recovery of major elements provide better selectivity and high recovery in downstream processing.

Thermodynamic analysis of the sulfation baking process illustrates that sulfuric acid starts to decompose in the temperature range of 127-427 °C, which corresponds to the permissible reaction temperature for sulfation. The sulfation reaction of Fe and Al is rapid and provides high extraction even at low processing temperatures, whereas the recovery of Ti and RE is highly restricted by kinetic limitations. The kinetic analysis of the sulfation process indicates that the reaction mechanism follows a product layer diffusion (Jander) model. The underlying activation energy for recovery of Ti and RE was found as 55.67 kJ/ mol and 42.11 kJ/mol, respectively. Furthermore, the dissolution trend indicates a strong correlation between Ti and RE extraction and are expected to be associated with each other in the crystal matrix. At the optimized sulfation conditions (300 °C, 1.3 mL/g acid, 1 h), approx. 90.1% Ti, 69.1% RE, 88.5% Al, 84.9% Fe, and 15.3% Si dissolution were obtained. The final residue consists of 70.92% SiO<sub>2</sub>, 10.29% TiO<sub>2</sub>, 7.42% Fe<sub>2</sub>O<sub>3</sub>, and 8.57% Al<sub>2</sub>O<sub>3</sub> and represent only 10.9 wt.% of the starting bauxite residue.

Approximately 91.12% Ti was recovered as TiO2 after thermal hydrolysis of the leach solution. The TiO<sub>2</sub> precipitate was characterized with high purity consisting of 99.76% TiO<sub>2</sub>, 0.20% Al<sub>2</sub>O<sub>3</sub>, 0.02% Fe<sub>2</sub>O<sub>3</sub>, and 0.03% SiO<sub>2</sub>. The leach solution was further subjected to crystallization to recover Al sulfate with high yield (94.5%) and purity (99.32% Al<sub>2</sub>(SO<sub>4</sub>)<sub>3</sub>, 0.31% TiO<sub>2</sub>, 0.35% Fe<sub>2</sub>O<sub>3</sub>, and 0.01% SiO<sub>2</sub>). The leach solution after Ti and Al recovery is composed of 6.46 ppm Sc, 17.91 ppm Y, 198 ppm Ce, and 0.85 ppm La as valuable components, along with 10.92 g/L Fe. Solvent extraction experiments using D2EHPA and Cyanex 272 show a positive response toward selective RE extraction. More than 85% RE were extracted into the organic phase using a 10 vol.% extractant diluted in kerosene at an O/A phase ratio of 1:1 within 15 min. The proposed flowsheet provides the dual benefit of high-volume reduction of bauxite residue and simultaneous recovery of major (Fe, Ti, Al) and minor (Sc, Y) components with high purity and yield.



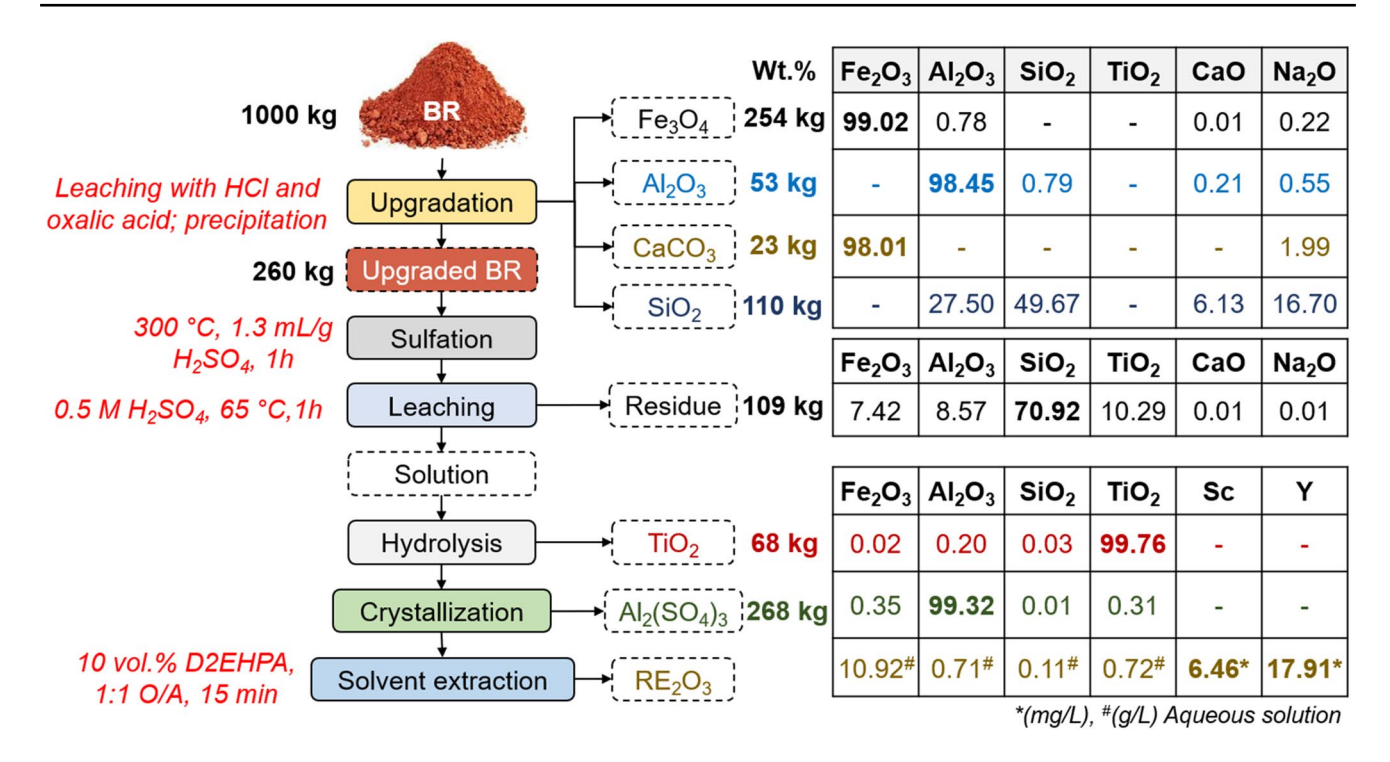


Fig. 11 Simplified flowsheet and material balance for high volume utilization of bauxite residue

**Acknowledgements** The authors are thankful to Mr. Glenn Yee for the fellowship he instituted at the Worcester Polytechnic Institute. Thanks are due to the NSF Center for Resource Recovery & Recycling for their technical support through Global Minerals Recovery, LLC.

#### **Declarations**

Conflict of interest The authors declare that they have no conflict of interest.

## References

- Habashi F (2016) A hundred years of the bayer process for alumina production. In: Donaldson D, Raahauge BE (eds.) Essential readings in light metals. Springer, Cham, pp. 85–93. https://doi.org/10.1007/978-3-319-48176-0\_12
- Healy S (2022) International Aluminum Institute, Sustainable Bauxite Residue Management Guidance 2022. https://international-aluminium.org/resource/sustainable-bauxite-mining-guide lines-second-edition-2022-2/
- Statistical annual report of USGS. U.S. Geological Survey, Mineral Commodity Summaries, "Aluminum" 2021. https://www.usgs.gov/centers/national-minerals-information-center/aluminum-statistics-and-information
- Evans K (2016) The history, challenges, and new developments in the management and use of bauxite residue. J Sustain Metall 2(4):316–331
- Di Carlo E, Boullemant A, Courtney R (2020) Ecotoxicological risk assessment of revegetated bauxite residue: Implications for future rehabilitation programmes. Sci Total Environ 698:134344

- Khairul MA, Zanganeh J, Moghtaderi B (2019) The composition, recycling and utilisation of Bayer red mud. Resour Conserv Recycl 141:483–498
- Ujaczki E et al (2018) Re-using bauxite residues: benefits beyond (critical raw) material recovery. J Chem Technol Biotechnol 93(9):2498–2510
- Borra CR et al (2016) Recovery of rare earths and other valuable metals from bauxite residue (red mud): a review. J Sustain Metall 2(4):365–386
- Mishra B, Gostu S (2017) Materials sustainability for environment: red-mud treatment. Front Chem Sci Eng 11(3):483

  –496
- Swain B, Akcil A, Lee J-C (2020) Red mud valorization an industrial waste circular economy challenge; review over processes and their chemistry. Critical Rev Environ Sci Technol 52:1–51
- Hammond K et al (2013) CR3 communication: red mud—a resource or a waste? Jom 65(3):340–341
- Abhilash, et al (2014) Extraction of lanthanum and cerium from Indian red mud. Int J Miner Process 127:70–73
- Agatzini-Leonardou S et al (2008) Titanium leaching from red mud by diluted sulfuric acid at atmospheric pressure. J Hazard Mater 157(2–3):579–586
- Agrawal S, Dhawan N (2021) Microwave acid baking of red mud for extraction of titanium and scandium values. Hydrometallurgy 204:105704
- Alkan G et al (2018) Novel approach for enhanced scandium and titanium leaching efficiency from bauxite residue with suppressed silica gel formation. Sci Rep 8(1):5676
- Borra CR et al (2016) Selective recovery of rare earths from bauxite residue by combination of sulfation, roasting and leaching. Miner Eng 92:151–159
- 17. Narayanan RP, Kazantzis NK, Emmert MH (2017) Selective process steps for the recovery of scandium from jamaican bauxite residue (red mud). ACS Sustain Chem Eng 6(1):1478–1488



- Borra CR et al (2015) Smelting of bauxite residue (red mud) in view of iron and selective rare earths recovery. J Sustain Metall 2(1):28–37
- Cardenia C, Balomenos E, Panias D (2018) Iron recovery from bauxite residue through reductive roasting and wet magnetic separation. J Sustain Metall 5(1):9–19
- Liu X et al (2020) Clean utilization of high-iron red mud by suspension magnetization roasting. Minerals Eng 157:106553
- 21. Kaußen F, Friedrich B (2015) Reductive smelting of red mud for iron recovery. Chem Ing Tec 87(11):1535–1542
- Mishra B, Staley A, Kirkpatrick D (2002) Recovery of valueadded products from red mud. Mining Metall Explor 19:87–94
- Azof FI et al (2020) The leachability of a ternary CaO-Al2O3-SiO2 slag produced from smelting-reduction of low-grade bauxite for alumina recovery. Hydrometallurgy 191:105184
- Erçağ E, Apak R (1997) Furnace smelting and extractive metallurgy of red mud: Recovery of TiO2, Al2O3 and pig iron. J Chem Technol Biotechnol 70(3):241–246
- Anawati J, Azimi G (2020) Recovery of strategic materials from canadian bauxite residue by smelting followed by acid bakingwater leaching. Springer International Publishing, Cham
- Archambo MS, Kawatra SK (2020) Utilization of bauxite residue: recovering iron values using the iron nugget process. Miner Process Extr Metall Rev 42(4):222–230
- Anawati J, Azimi G (2022) Integrated carbothermic smelting

   acid baking water leaching process for extraction of scandium, aluminum, and iron from bauxite residue. J Cleaner Prod 330:129905
- 28. Tanvar H, Mishra B (2021) Hydrometallurgical recycling of red mud to produce materials for industrial applications: alkali

- separation, iron leaching and extraction. Metall and Mater Trans B 52:3543-3557
- US Patent US1504672A. Preparation of titanium hydroxide. Inventor: Joseph Blumenfeld, https://patents.google.com/patent/ US1504672A/en
- Grzmil BU, Grela D, Kic B (2008) Hydrolysis of titanium sulphate compounds. Chem Pap 62(1):18–25
- Schwartz D et al (2000) A kinetic study of the decomposition of spent sulfuric acids at high temperature. Ind Eng Chem Res 39(7):2183–2189
- Han KN, Rubcumintara T, Fuerstenau MC (1987) Leaching behavior of ilmenite with sulfuric acid. Metall Trans B 18(2):325–330
- Dubenko AV et al (2020) Mechanism, thermodynamics and kinetics of rutile leaching process by sulfuric acid reactions. Processes 8(6):640
- Coats AW, Redfern JP (1964) Kinetic parameters from thermogravimetric data. Nature 201(4914):68–69
- Tanvar H, Mishra B (2022) Comprehensive utilization of bauxite residue for simultaneous recovery of base metals and critical elements. Sustain Mater Technol 33:e00466

**Publisher's Note** Springer Nature remains neutral with regard to jurisdictional claims in published maps and institutional affiliations.

Springer Nature or its licensor (e.g. a society or other partner) holds exclusive rights to this article under a publishing agreement with the author(s) or other rightsholder(s); author self-archiving of the accepted manuscript version of this article is solely governed by the terms of such publishing agreement and applicable law.

